metals

MDPI

Article

The Effect of Deformation and Isothermal Heat Treatment of a 5005 Aluminum Alloy

Jon Holmestad [1,*], Calin Daniel Marioara [2], Benedikte Jørgensen Myrold [1] and Ola Jensrud [1]

[1] SINTEF Manufacturing AS, 2830 Raufoss, Norway; benedikte.myrold@sintef.no (B.J.M.); ola.jensrud@sintef.no (O.J.)
[2] SINTEF Industry, 7465 Trondheim, Norway; calin.d.marioara@sintef.no
* Correspondence: jon.holmestad@sintef.no

Abstract: In the aluminum industry, forming is an important process step that introduces dislocations in the material. To investigate the effect of dislocation retention after ageing on 6xxx-series alloys, a non-heat-treatable 5005 alloy was selected to measure the change in mechanical properties due to dislocation annihilation during dynamic recovery. However, the isothermal ageing treatment led to an unexpected and significant increase in mechanical properties after deformation. Increases in yield strength of 120% and tensile strength of 50% compared with the as-received material were achieved. However, this caused a significant decrease in elongation properties. The deformation start temperature did not have any impact on the final mechanical properties. TEM analysis attributed the increase in mechanical properties to an increased precipitation and dislocation density compared with the undeformed reference material. The precipitates are located along dislocation lines, showing that the solute elements are preferentially segregating to dislocations and precipitating. The precipitates were typical for the Al–Mg–Si(–Cu) system; therefore, the low amounts of Si and, to a lesser extent, Cu were responsible for the precipitation hardening in the 5005 alloy.

Keywords: artificial ageing; 5xxx aluminum alloy; forming; deformation; mechanical properties; precipitates

Citation: Holmestad, J.; Marioara, C.D.; Myrold, B.J.; Jensrud, O. The Effect of Deformation and Isothermal Heat Treatment of a 5005 Aluminum Alloy. *Metals* **2024**, *14*, 225. https://doi.org/10.3390/met14020225

Academic Editors: Atef Saad Hamada and Ruizhi Wu

Received: 8 December 2023
Revised: 26 January 2024
Accepted: 6 February 2024
Published: 12 February 2024

1. Introduction

Both 5xxx- and 6xxx-series aluminum are extensively used in the automotive industry due to their excellent strength-to-weight ratio, good corrosion resistance, and good formability [1]. The 5xxx series is non-heat-treatable, and strength is gained mainly from solid solution and strain hardening [2]. However, in 6xxx-series alloys, strength is gained mainly through precipitation hardening during artificial ageing [3].

The precipitation sequence in 6xxx-series alloys has been extensively studied and is well known. The main hardening phase is the coherent needle-shaped β″, but during overageing, more stable semicoherent precipitates are formed [4]. When the Mg–Si ratio is varied, several different types of ordered and disordered particles will precipitate [5]. All the metastable precipitates have one full coherency direction with the <100>Al directions in the face-centered cubic Al matrix. For this reason, they take needle/rod/plate morphologies with elongation in one <100>Al direction. It means that the atoms in their structures arrange in cross section on two planes with $a_{Al}/2$ = 2.025 Å separation, each plane having a_{Al} = 4.05 Å periodicity along the needle length. Different precipitate types have different atomic arrangements on the two planes, which give variable symmetries and compositions of the metastable phases. It was recently discovered that all the metastable precipitates are connected by a set of common construction rules, which dictate that each Al atom must have 12 near neighbor atoms, each Mg 15, and each Si 9 [6]. The consequence of these rules is that when viewed in projection along the needle length, each Al atomic column in the cross section will sit in a fourfold symmetry in respect to the nearest neighbor

atomic columns, each Mg column will sit in a fivefold symmetry, and each Si in a threefold symmetry [7]. Each Al column will be surrounded by four near columns with opposite heights (located on the other plane), each Mg by five, and each Si by three near columns of opposite heights. In Cu-containing alloys, Cu atomic columns can take both threefold and fourfold symmetries when partly replacing Al columns in the interfaces of precipitates with the matrix [8]. The consequence of these rules is that an exact atomic overlay can be made on two-dimensional Z-contrast atomic-resolution high-angle annular dark-field scanning transmission electron microscopy (HAADF-STEM) images of precipitate cross sections, enabling their full characterization. Another consequence of the rules is that the projected positions of the Si atomic columns in the precipitate cross-section plane are nearly hexagonal with a projected separation of approximately 4 Å. This has been named 'the Si-network' and provides a structural connection between the different precipitate structures [9].

Recent works have shown that precipitation hardening can occur in 5xxx-series aluminum alloys if Zn [10,11] is added. Increased mechanical properties were observed after cold rolling and ageing in a 5083 alloy with 2 wt% Zn, with an effect of both the work and precipitation hardening [10]. A nonisothermal heat treatment of the 5083 alloy showed increased mechanical properties, enhanced ageing kinetics, and improved corrosion resistance [11]. However, the increased mechanical properties depended on the choice of heat treatment.

An Al–3Mg alloy with Cu showed the presence of GPB (Guinier–Preston–Bagaryatsky) zones after paint baking similar to what has been found in 2xxx-series aluminum alloys [12]. However, a significant hardening occurred even though the Cu additions in this alloy (<0.1 at%) was much lower than what is commonly found in Al–Cu–Mg alloys (>1 at%) [13].

β-Mg_3Al_2 can precipitate during sensitization of the alloys, but this can cause increased susceptibility to corrosion [14] and does not have much impact on mechanical properties [15]. It has been shown that the heat treatment of 5083-H116 [2], an alloy containing more solute Mg than the alloy investigated in this paper, can lead to a reduction in mechanical properties due to the precipitation of β-Mg_3Al_2 on grain boundaries, and lead to less solid solution hardening of the material.

Prestraining (cold rolling reduction) increased the number of nucleation sites and influenced the precipitation kinetics of β-Mg_3Al_2 precipitates. [16]. Heterogeneous precipitation with a shorter distance between precipitates than in the nonstrained material was observed.

The precipitation of β-Mg_3Al_2 has been modelled and experimentally investigated in tempers with a different strain hardening, i.e., different cold rolling reduction [17]. The nucleation and coarsening rates of the precipitates were different in the investigated tempers.

Increased mechanical properties were found during high-pressure heat treatment in a 5005 alloy [18]. This increase was attributed to a refinement of grains during the process.

The dislocation density of an alloy after forming can be measured in various ways [19], both directly and indirectly. The direct ways are complicated and require advanced scientific equipment, but the effect of the dislocations on macroscopic properties can be measured more easily. It is well known that dislocations prevent the motion of other dislocations, hence increasing the yield and tensile strength of the material [20]. The increase or reduction in dislocations can therefore be measured by the mechanical properties if no other hardening effect is present.

The deformation temperature has an impact on dynamic recovery during deformation [21]. Deformation at cryogenic temperatures was performed, and the yield, tensile, and elongation were improved compared with room temperature deformation. This increase in mechanical properties was attributed to a reduction in dynamic recovery after deformation at cryogenic temperatures and a higher dislocation density in the material.

In a 6xxx-series alloy, precipitation occurs, and the dislocation density cannot be inferred by measuring the mechanical properties. This work-hardening effect has been investigated and modelled [22,23]. The effect of deformation at both room temperature and

elevated temperatures in a 6xxx aluminum alloy has been investigated, and deformation at elevated temperatures leads to a reduction in mechanical properties [22]. The authors attributed this decrease to a lower efficiency to store dislocations, as well as to dynamic recovery. Khadyko et al. [23] proposed a crystal plasticity and precipitation model for the precipitation and work hardening of 6XXX alloy, which showed good predictions of relative changes in work hardening, but was inaccurate for early states of ageing as it did not account for the incubation time.

In recent years, hot die quenching during deformation has been developed to produce components with high ductility and with the potential of excellent mechanical properties after artificial ageing [24]. The hot stamping-in-die quenching process has been found to increase the yield strength of a 5083 alloy, while the elongation was slightly reduced [25]. Finite element simulation showed that the hot stamping process was more suitable for the formation of skin when compared with hot drawing.

The hot form quenching of a 7055 aluminum alloy combined with preageing and simulated baking (ageing) was found to increase the mechanical properties by 10% compared with similar alloys as the precipitate sequence could be manipulated to increase the number density of strengthening η'-precipitates [26]. In a 7075 aluminum alloy, the increased dislocation density after hot form quenching leads to an increased precipitation density and an increased strengthening contribution from dislocations and precipitation despite a slight reduction in solid solution strengthening [27].

Based on these considerations, an idea to experimentally measure the dislocation density was to use a non-heat-treatable 5005 alloy to measure the effect of the isothermal heat treatment on the mechanical properties and, hence, infer if there is a reduction in dislocation density due to dynamic recovery. In an alloy where no precipitation occurs, the changes in mechanical properties during isothermal heat treatment will be closely linked to the dislocation density of the material.

As an unexpected increase in mechanical properties was found in the 5005 alloy after isothermal heat treatment, the focus became to understand the reason for this increase and to investigate whether precipitates, and what type, were formed during the isothermal heat treatment.

2. Materials and Methods

A 5005 rolled aluminum sheet with the alloy composition given in Table 1 was used for the experiments. The main alloying element was Mg, but small amounts Si, Fe, Cu, Mn, and Ti were also present in the alloy.

Table 1. The alloy composition of the investigated alloy.

Alloy	Si (wt%)	Fe (wt%)	Cu (wt%)	Mn (wt%)	Mg (wt%)	Ti (wt%)	Al (wt%)
Alloy A	0.15	0.26	0.02	0.02	0.87	0.015	Balance

The alloy sheet with a thickness of 5.4 mm was cut into blanks with an area of 150 × 25 mm, with the longitudinal direction parallel to the rolling direction. The blanks were heated to 565 °C in an air circulation furnace and kept at this temperature for 10 min. The blanks were then cooled by different methods to a predefined target temperature before insertion into a flat deformation tool attached to a 300-ton hydraulic press. The blanks were compressed from 5.4 mm to approximately 4.7 mm, giving a thickness reduction of 13%. The deformation tool was kept at room temperature during the entire experiment, and the blank was quenched in the tool to room temperature, a.k.a. hot form quenching [24].

Cooling to the deformation temperature was performed both with water quenching for rapid cooling to room temperature and with a cooling tool made of steel plates that allowed rapid and controlled cooling to a desired temperature. The deformation temperatures investigated are given in Table 2, where 500 °C was the highest temperature

that could be reached due to air cooling during the transportation of the blank from the furnace to the press. The cooling rates and times for the different cooling media to the selected temperatures were measured repeatedly with a thermocouple on blanks before the experiment, and a stopwatch was used to determine the end of cooling based on this during the experiment. To reach the intermediate deformation temperature of 250 °C, the time in the cooling tool was 8 s. The cooling tool was kept at a temperature of 100 °C to sufficiently reduce the cooling rate to be able to control the end cooling temperature.

Table 2. Overview of the investigated deformation temperature, cooling methods, and legend used.

Name of Condition (Legend)	High (H)	Intermediate (IM)	Intermediate Deformed (IM Def)	Room Temperature (WQ)	Undeformed (Undef)	As Received (Rec)
Deformation Temperature (°C)	500	250	250	25	undeformed	Undeformed
Cooling method	No cooling	Cooling tool	Cooling Tool	Water quenched	Water quenched	Not heat treated
Artificially aged	Isothermal	Isothermal	No	Isothermal	Isothermal	No

An undeformed blank went through the solution heat treatment, but was water-quenched before artificial ageing to be able to observe the effect of no deformation on the final mechanical properties.

The blanks were then isothermally heat-treated at 185 °C for 3 h to obtain the final temper before they were machined to tensile test specimens and tested according to ISO 6892-1:2019 [28] in a Zwick Z250 tensile testing machine (ZwickRoell GmbH, Ulm, Germany). Three parallels in each condition were tested to obtain the mechanical properties. Both the deformed and undeformed tensile test samples were oriented along the rolling direction of the original sheet material.

One set of blanks, intermediate deformed (IM Def), was not isothermally heat-treated, so the effect of the heat treatment on the mechanical properties can also be investigated. The thermomechanical treatment and the labelling of all conditions produced for this work are listed in Table 2 and shown schematically in Figure 1.

The intermediate (IM) and undeformed (Undef) conditions were, based on the mechanical properties, selected to be more thoroughly investigated.

The samples were cast in epoxy, ground, and polished before investigating in an optical microscope. The grain structure was obtained by using polarized light after the sample had been anodized in Barker's reagent (HBF_4) at 40 V for 60 s with Struers LectroPol-5 (Struers ApS, Ballerup, Denmark).

A JEOL JEM 2100 TEM (transmission electron microscope) (JEOL, Tokyo, Japan) was used to determine the precipitate microstructure present after the artificial aging in the IM and Undef conditions. The microscope has a LaB_6 gun and was operated at 200 kV. It is equipped with a Gatan imaging filter (GIF) that enables the measurement of specimen thickness corresponding to recorded bright-field (BF) and dark-field (DF) images by electron energy loss spectroscopy (EELS) (Gatan, Inc., Pleasanton, CA, USA). The precipitates found were of the type typical for Al–Mg–Si(–Cu) alloys with needle morphology along the crystallographic <100>Al directions. Therefore, a methodology described in [5] was used to determine their parameters, such as volume density, average needle length, cross section, and volume fraction. A total of 12 bright-field images and their corresponding dark-field images were recorded with the matrix oriented along <001>Al from each condition, and the specimen thickness in each image was measured by EELS to determine the precipitate volume density. The measured thicknesses were between 70 and 130 nm with an average of approximately 110 nm in each condition. The lengths of 380 needles in the Undef condition and 610 needles in the IM condition were measured to determine the average needle length. In addition to the abovementioned images, 20 bright-field images at higher magnifications from the Undef condition and 37 from the IM condition were recorded to measure the

precipitate's cross-section areas. A total of 44 cross sections were measured from the Undef condition, and 229 from the IM condition.

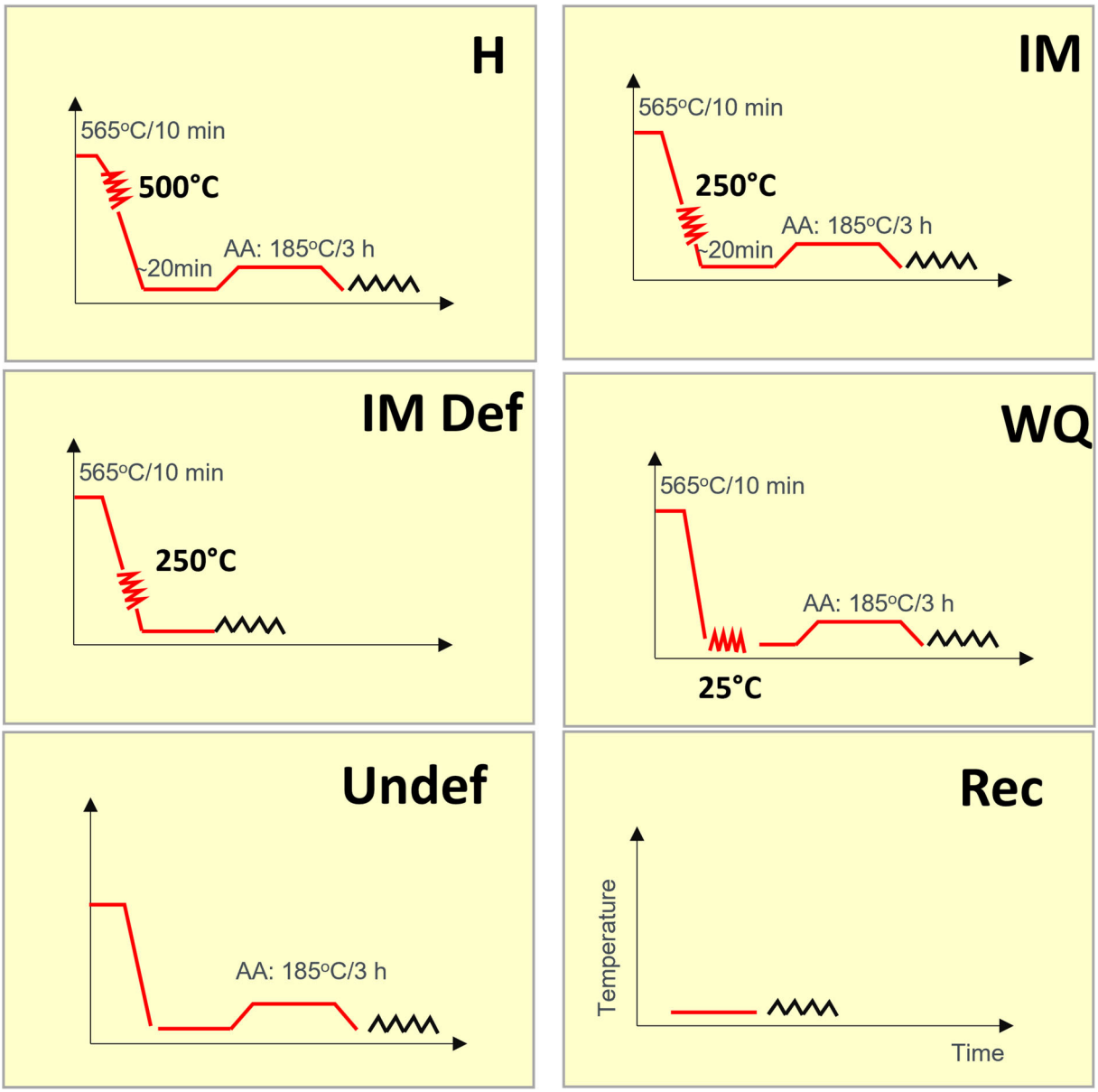

Figure 1. The thermomechanical treatment of the conditions produced in this work. H, IM, and WQ show deformation after solution heat treatment and before artificial ageing. IM Def shows deformation after solution heat treatment without artificial ageing, while the Undef condition is solution-heat-treated and artificially aged without deformation. Finally, the Rec condition is only tested without any additional thermomechanical processing. Deformation is shown with red serrations, and mechanical testing with black serrations.

The precipitate types were determined by Z-contrast, atomic-resolution HAADF-STEM (high-angle annular dark-field scanning transmission electron microscopy) imaging using a probe Cs-corrected JEOL JEM-ARM200F operated at 200 kV. The probe size was 0.1 nm, the convergence semi-angle was 27.42 mrad and the inner and outer collection angles were 51 and 203 mrad, respectively. All HAADF-STEM images shown in this work were taken with the grains oriented along a <001>Al direction.

TEM samples were prepared from cross sections along the rolling direction, i.e., the long direction of the deformed blanks. They were ground to thin foils of about 100 mm

thickness with successively finer grinding paper up to #4000 grit. Samples with Ø3 mm were stamped out and electropolished in a Struers TenuPol-5 unit with the electrolyte (1/3 nitric acid + 2/3 methanol) kept at −20 °C.

3. Results

3.1. Mechanical Properties

The mechanical properties of the investigated conditions are shown in Figure 2 with the actual values shown in Table 3. There are no significant differences in yield (YS) or tensile strength (UTS) among the alloys that have been deformed. However, there is a significant increase in both yield and tensile strength compared with the undeformed and as-received condition. The yield strength is increased by 70–80 MPa, while the ultimate tensile strength is increased by 50–60 MPa. The undeformed sample shows only small variations in yield and tensile strength compared with the as-received sample.

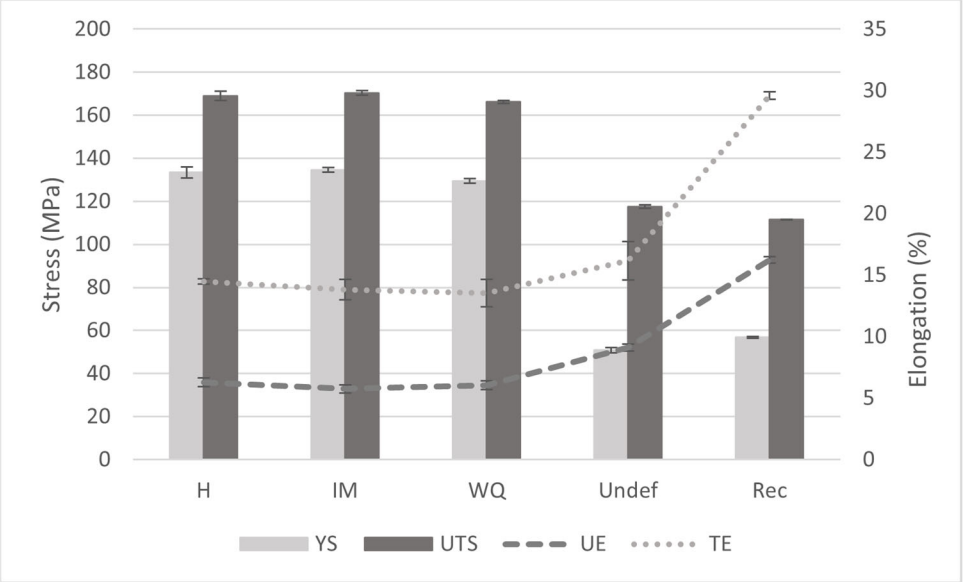

Figure 2. Mechanical properties of the investigated artificially aged and as-received conditions.

Table 3. Mechanical properties of the selected conditions.

Condition	Yield Strength (MPa)	Ultimate Tensile Strength (MPa)	Uniform Elongation (%)	Total Elongation (%)
H	133 ± 2.5	169 ± 2.1	6 ± 0.36	14 ± 0.20
IM	135 ± 1.2	170 ± 1.1	6 ± 0.34	14 ± 0.83
IM Def	117 ± 1.7	125 ± 1.2	1 ± 0.13	10 ± 0.36
WQ	130 ± 1.1	166 ± 0.8	6 ± 0.33	14 ± 1.10
Undef	51 ± 1.2	118 ± 0.82	9 ± 0.30	16 ± 1.55
Rec	57 ± 0.5	111 ± 0.2	16 ± 0.25	30 ± 0.3

On the other hand, the elongation decreases in the deformed conditions compared with the undeformed and as-received samples. There is only a slight decrease in elongation of the deformed conditions compared with the undeformed condition, but large decreases of 10% in uniform elongation (UE) and 16% in total elongation (TE) compared with the as-received material. The deformation temperature does not appear to have an impact on the tensile or elongation properties with all deformed samples showing very similar elongation properties.

The effect of artificial ageing after deformation is shown in Figure 3, where the mechanical properties are increased after artificial ageing. There are increases in yield strength of 18 MPa, ultimate tensile strength of 45 MPa, uniform elongation of 5%, and total elongation

of 4%. However, the intermediate deformed condition shows increased yield and ultimate tensile strength compared with the undeformed and as-received samples. Therefore, an effect on mechanical properties both from the deformation and from the artificial ageing has been measured.

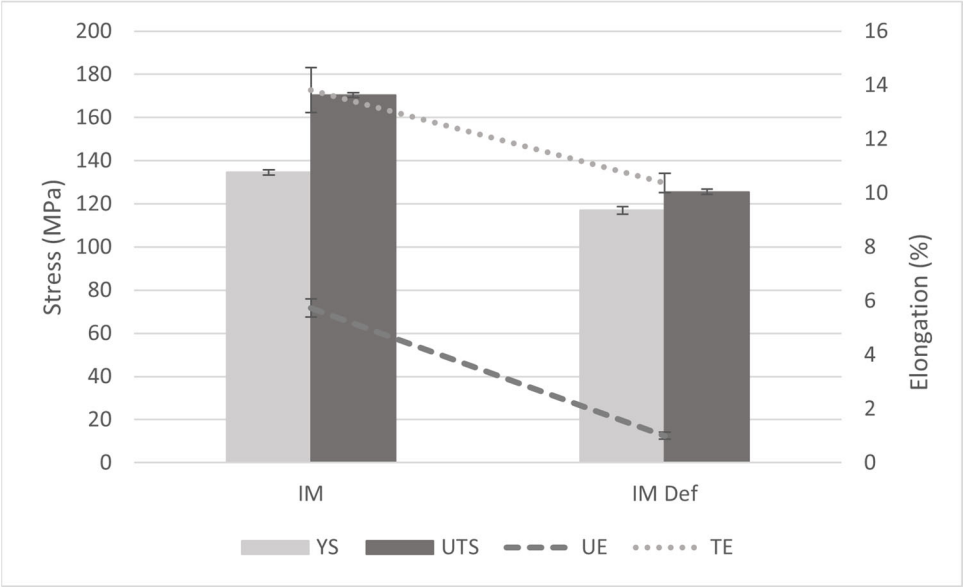

Figure 3. Mechanical properties showing the effect of isothermal artificial ageing after deformation. The artificial ageing increases the yield strength, tensile strength, uniform elongation, and total elongation of the material after deformation at 250 °C.

Representative stress–strain curves of the IM, IM def, and Undef conditions are shown in Figure 4, visually showing the significant differences due to artificial ageing (IM vs. IM def) and due to deformation (IM vs. Undef). The Portevin–Le Chatelier effect is observed in the tensile tests.

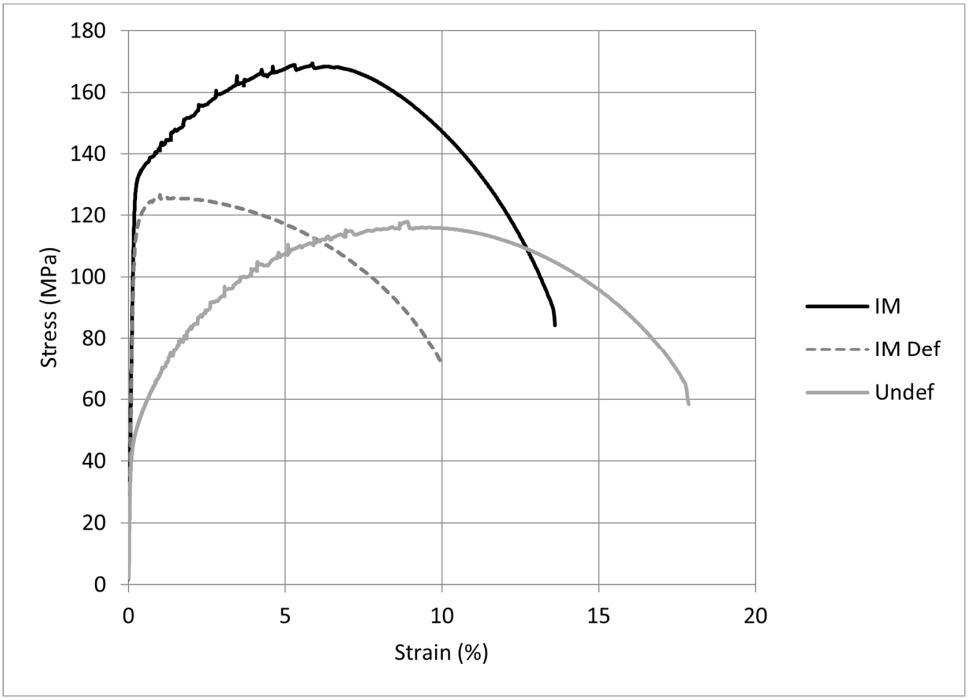

Figure 4. Nominal stress–strain curves of the selected conditions.

3.2. Optical Microscopy

Optical micrographs showing the structure of the IM and Undef conditions are shown in Figure 5. The primary particles are broken up along the rolling direction, but there are no significant visible differences between the conditions due to the deformation.

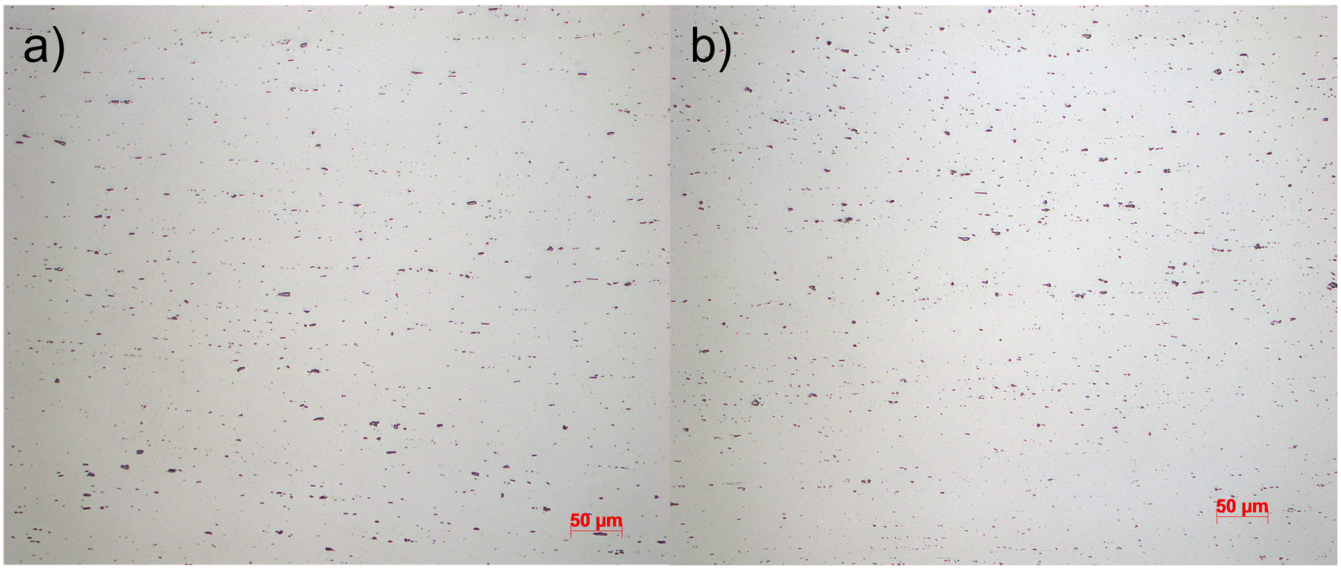

Figure 5. Optical micrographs of the IM (**a**) and Undef (**b**) conditions. The rolling direction is in the horizontal direction.

The grain structure is shown in Figure 6. There are no significant changes after the deformation, with a recrystallized structure visible in both the IM and Undef conditions.

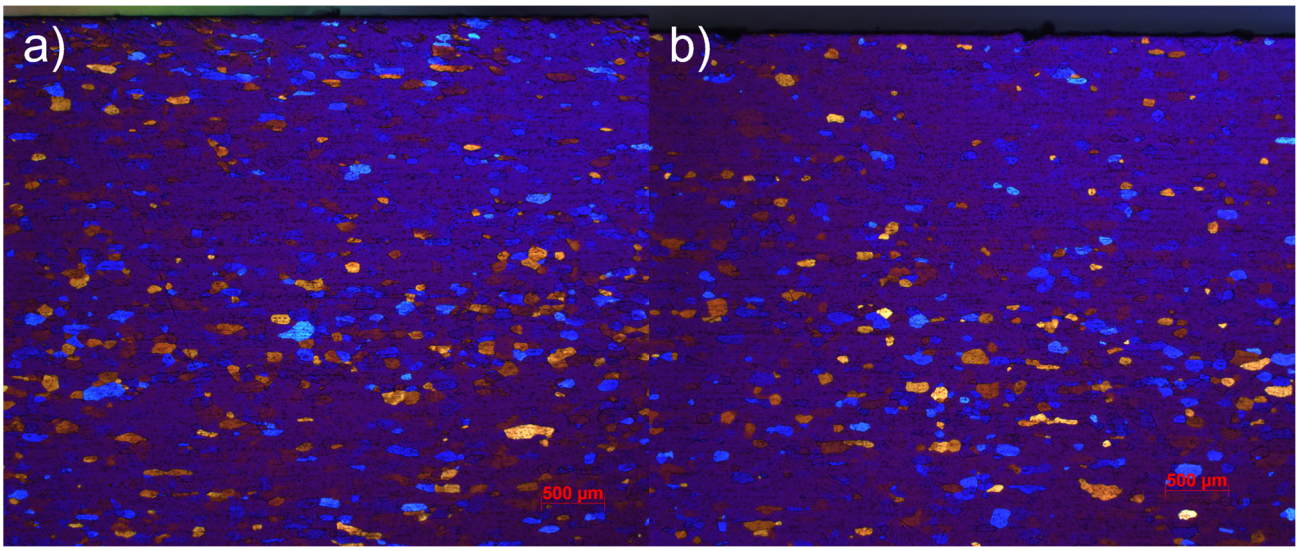

Figure 6. Anodized micrographs of the IM (**a**) and Undef (**b**) conditions. The rolling direction is in the horizontal direction.

3.3. Precipitate Microstructure

The precipitate microstructure is shown in Figure 7. There is a clear difference between the IM and Undef conditions. In the intermediate condition, the precipitates are denser and more inhomogeneously distributed, with most of them located on dislocation lines. Many areas in between the dislocations are void of any visible precipitation. In the undeformed condition, the precipitation density is lower, and the precipitates are more homogeneously distributed in the aluminum matrix.

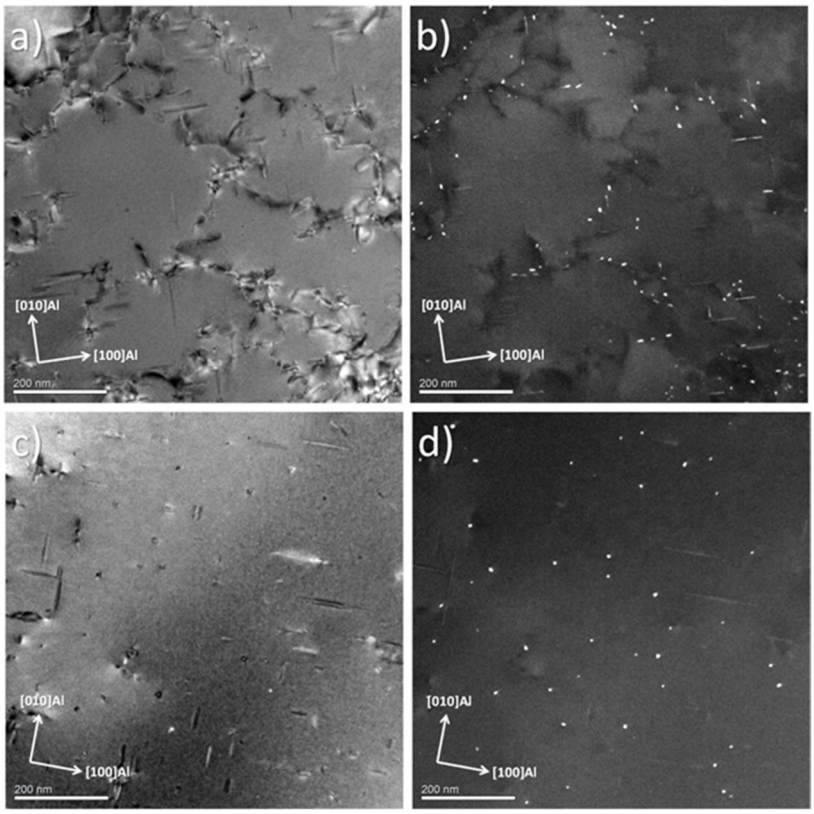

Figure 7. (**a**) Bright-field TEM image of the IM condition and (**b**) its corresponding dark-field image; (**c**) bright-field image of the Undef condition and (**d**) its corresponding dark-field image. Two-thirds of the precipitates are observed perpendicular (as needles) in the bright-field images, and 1/3 in the cross section (as bright dots) in the dark-field images. The crystallographic orientation of the matrix is indicated. The measured thicknesses of the specimen were 118 nm for the IM condition and 106 nm for the Undef condition.

Figure 7 also shows that the dislocation density in the Undeformed condition is much lower than in the deformed sample, with multiple dislocation lines visible in the IM condition, while the Undef condition doesn't have any clearly visible dislocation lines.

The precipitate statistics shown in Table 4 indicate that the intermediate condition has approximately four times as many precipitates with slightly shorter needle lengths, but a similar cross-section size as the undeformed condition, leading to a volume fraction that is three times that of the undeformed condition.

Table 4. The precipitate statistics of the investigated conditions.

Condition	Needle Density (μm^{-3})	Needle Length (nm)	Cross Section (nm^2)	Volume Fraction (%)
IM	3841 ± 411	34.14 ± 0.68	14.78 ± 0.54	0.194 ± 0.023
Undef	1018 ± 200	41.24 ± 1.51	15.15 ± 0.82	0.064 ± 0.013

3.4. Precipitate Types

Analysis of the high-magnification bright-field images used to measure precipitate cross-section areas indicated that most of the precipitates in the undeformed condition were disordered overall, without a clear periodicity; see Figure 8a–c. Some precipitates had a periodicity of approximately 7 Å consistent with the β′ phase (see Figure 8d,e), while a low fraction showed a cross-section shape and periodicity consistent with the β″ phase; see Figure 8f.

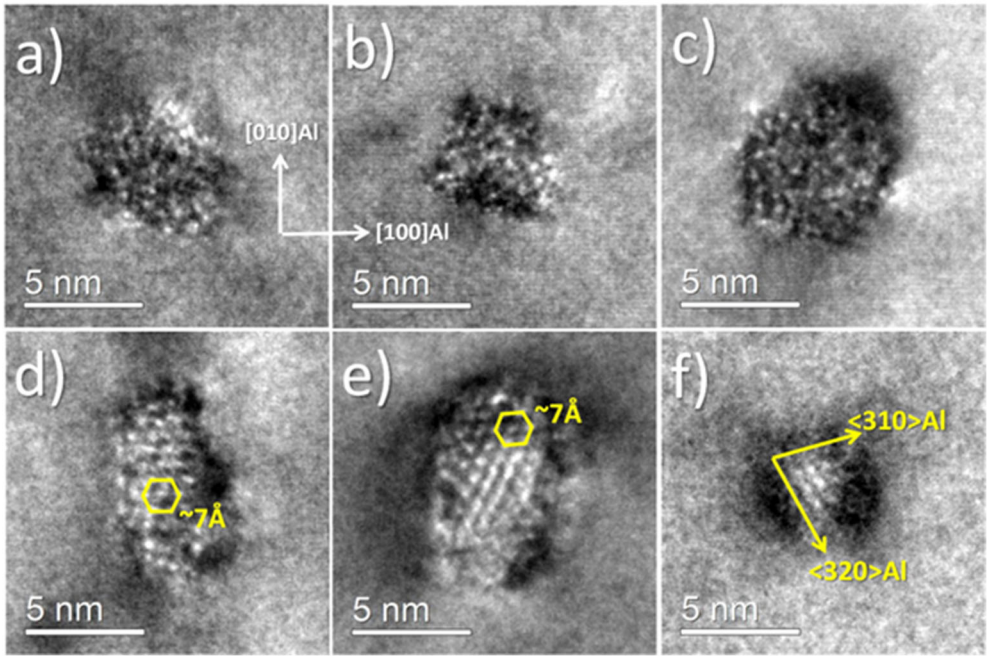

Figure 8. Bright-field images of precipitate cross sections in the undeformed condition. (**a**–**c**) show disordered precipitates, and (**d**,**e**) show periodicities consistent with the β′ phase, while (**f**) shows a cross-section shape consistent with the monoclinic β″ phase.

As the IM condition of the investigated 5xxx alloy showed a strong precipitation hardening response due to the formation of Al–Mg–Si(–Cu)-type precipitates preferentially along dislocation lines, it was decided to investigate these precipitates in higher detail. For this purpose, they were imaged with the Z-contrast, atomic-resolution HAADF-STEM technique. Here, each dot represents a projected atomic column having ~100 atoms for a specimen thickness of approximately 40 nm. The face-centered cubic (FCC) Al matrix viewed along a <001>Al projection has a square pattern in projection with a separation of $a_{Al}/2$ = 2.025 Å, while the precipitates are viewed in cross section along their needle lengths. The atomic overlay is based on the construction rules from [6], the established knowledge about the crystal structure of precipitates in the Al–Mg–Si(–Cu) system [7], and on the Z-contrast of atomic columns in the images.

According to the morphology of their cross section, the precipitates nucleated on dislocations were classified as discrete needle or rod shaped, with a well-defined cross section, and as decorating, with a continuous cross section following the dislocation line. Figures 9 and 10 give two examples of discrete precipitates. The precipitate in Figure 9 can be classified as a typical β′ phase with structure defined in Table 6 in reference [29], where, for better clarity, Si2a and Si2b sites are renamed Si2 and Si3, respectively. However, the orientation of its cross section and Si-network is along <100>Al, similar to the L-phase and C-plate [8]. Atomic columns with a strong contrast are observed periodically along this direction at the interface of the precipitate with the Al matrix. The separation between these columns is $3d_{Al}$ (12.15 Å) and $4d_{Al}$ (16.20 Å). It indicates that the bright columns contain Cu, and this is the same type of interface present in the C-plate and β′ phase forming in Cu-containing, Mg-rich alloys [8,30]. The electron density map in [30] shows that a strong covalent bonding forms between the Cu atoms at the interface and the adjacent Si atoms that are part of the Si-network. This bonding gives rise to a well-defined unit present in precipitates with this type of interface, named C subunit in [8].

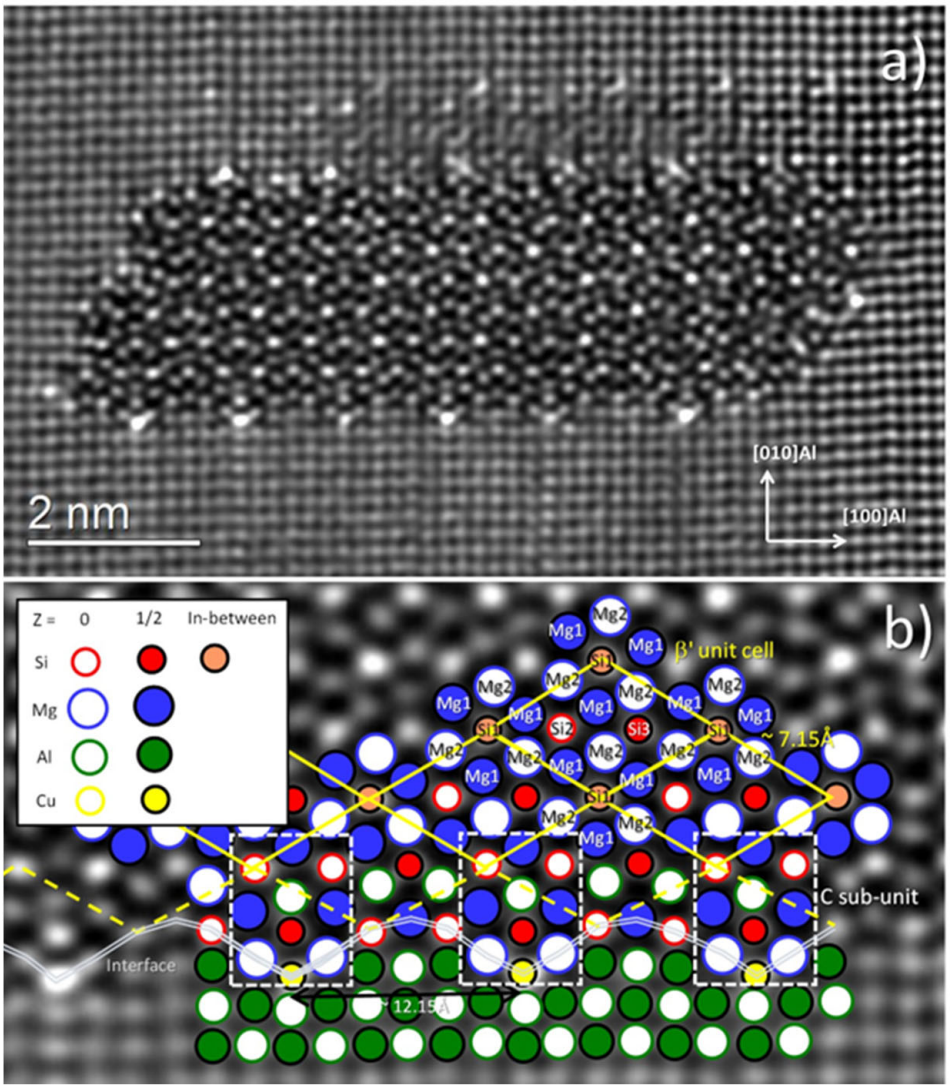

Figure 9. HAADF-STEM image of a β′ phase in the IM condition: (**a**) overview image; (**b**) zoomed-in lower side with atomic overlay. The atomic sites in the β′ phase are labelled according to [29]. The β′ unit cell is drawn with yellow lines. The C subunit is identified according to [8] and drawn with dashed white lines. The interface between the precipitate and the matrix is marked by gray double lines, and its periodicity is indicated. The matrix orientation shown in (**a**) and the legend in the upper-left side of (**b**) are also used in Figures 10–12.

The precipitate in Figure 10 is formed at the end of a dislocation line and displays a periodicity consistent with a β′ phase. However, a close analysis of its crystal structure reveals that it is of a different type from the precipitate shown in Figure 9. The unit cell marked with yellow lines in Figure 10 is isostructural with a β′Ag phase, as defined in [31]. This structure can also form in Cu-containing alloys, with Cu replacing Ag in the unit cell [8]. It is interesting to note that the Ag/Cu atomic sites at the corners of the β′Ag unit cells in Figure 10 do not have a brighter contrast than the Cu-containing columns at the precipitate interface with the Al matrix, which indicates that they are occupied by Si. This makes sense, as the Ag/Cu sites in the β′Ag phase are part of the Si-network. This precipitate has two structurally different interfaces with the matrix along <110>Al and <310>Al, as indicated in Figure 10a.

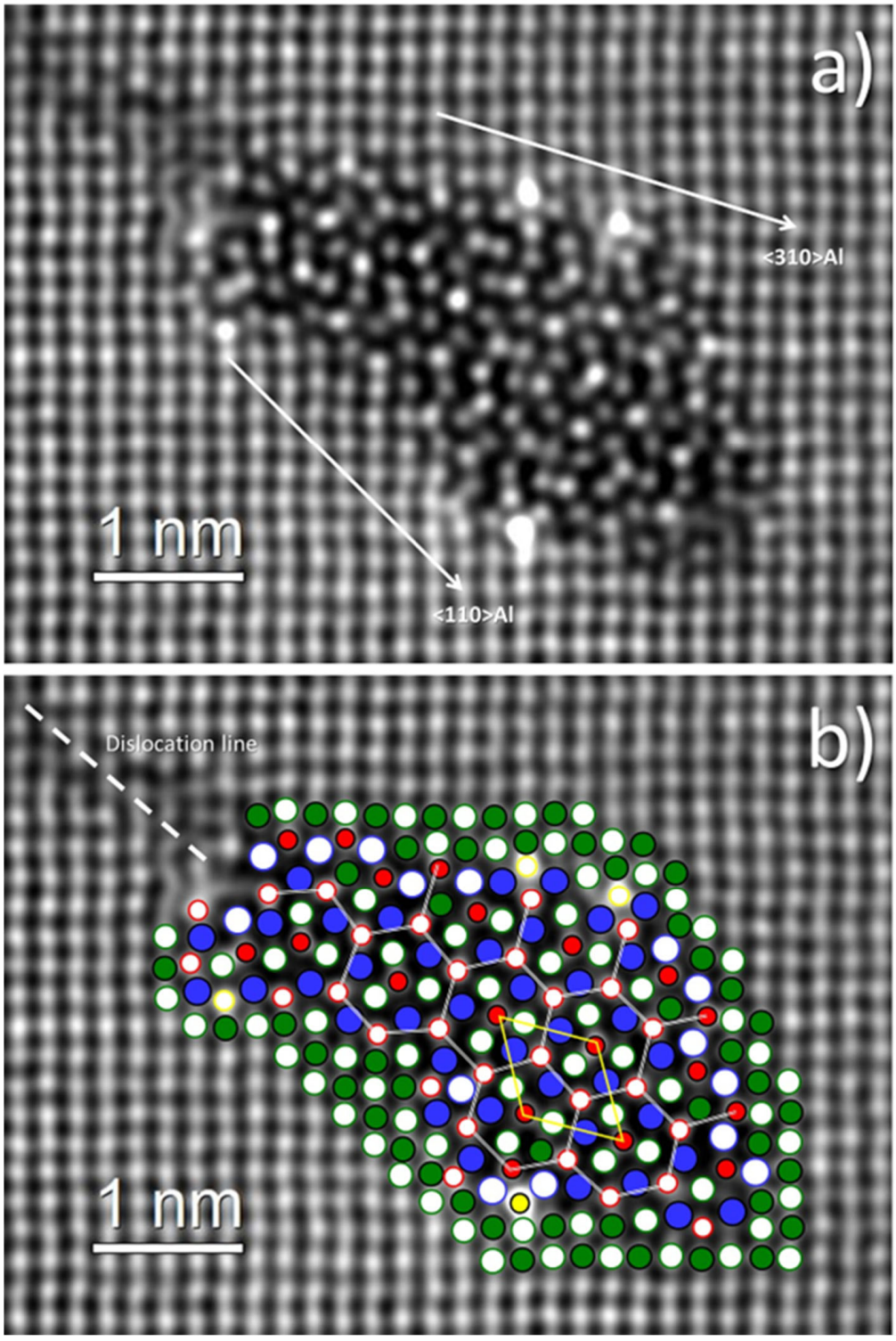

Figure 10. HAADF-STEM image of a precipitate isostructural with a β'_{Ag} phase, where the Ag sites at the corners of unit cells are occupied by Si: (**a**) overview image; (**b**) atomic overlay. The directions of the precipitate's interface with the Al matrix are indicated in (**a**). In (**b**), one β'_{Ag} unit cell is drawn with yellow lines, and the Si atomic columns corresponding to the β'_{Ag} phase are connected with white double lines.

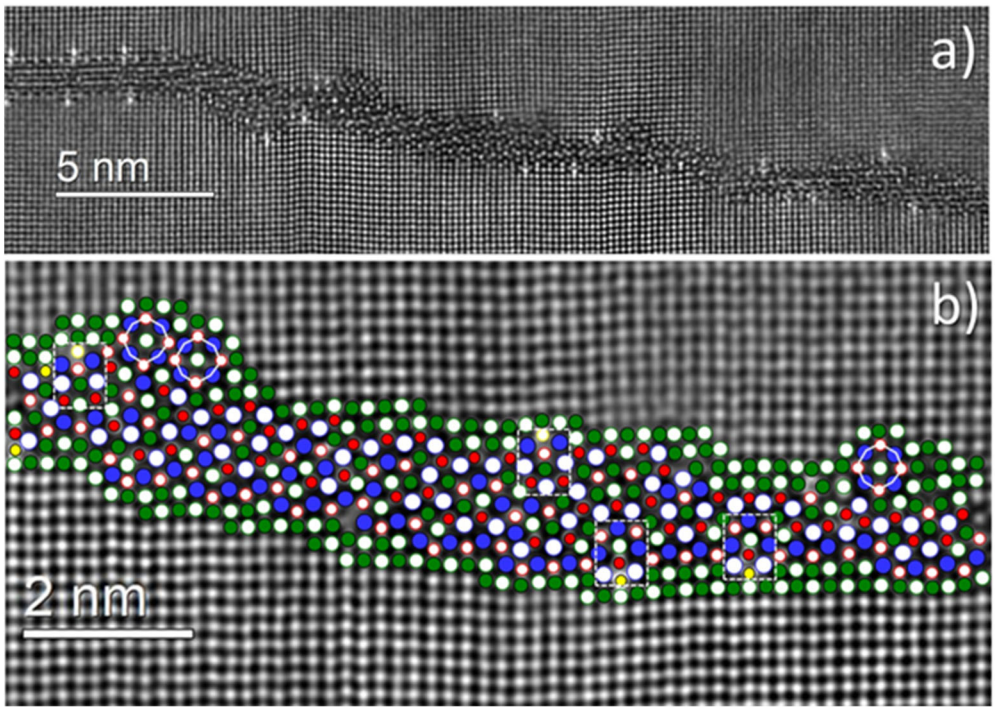

Figure 11. HAADF-STEM image of a precipitate decorating a dislocation line: (**a**) overview; (**b**) atomic overlay of the central part of the precipitate. C subunits are indicated by dashed white lines, and β″ structural units (eyes) are indicated by continuous white lines.

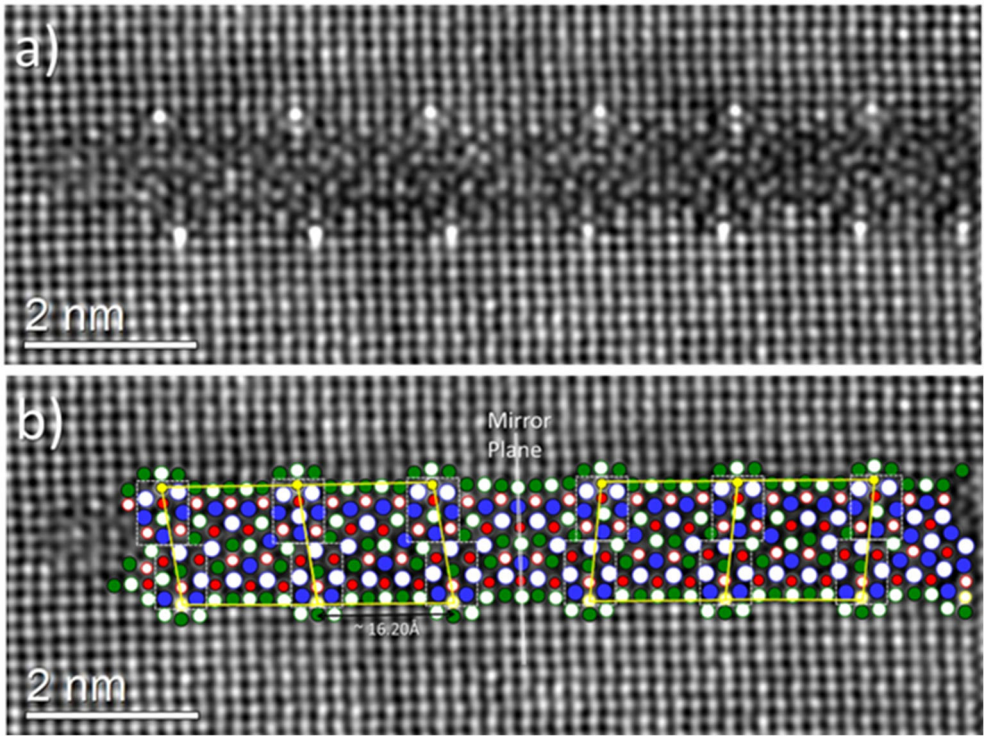

Figure 12. HAADF-STEM image of a precipitate decorating a dislocation line: (**a**) overview; (**b**) with atomic overlay. It consists of a monoclinic unit drawn with yellow lines that contains C subunits indicated by white dashed lines. The whole structure is mirrored by a mirror plane indicated by the double white line.

Figure 11 shows a precipitate decorating a dislocation line. Atomic overlay was performed in the central part of it, where the precipitate was in focus and the individual atomic

columns could be imaged. It shows no periodicity, although it contains the hexagonal Si-network throughout its entire length. It is interesting to note that a few Cu atomic columns are present at the interface with local orientation along <100>Al, and in these locations, each Cu column generates one C subunit, as indicated. It becomes clear that such units stabilize the interface and help accommodate the lattice misfit. Three eyelike structural units of the peak hardening β″ phase [6,8] are also present on the upper interface with the matrix, which is unusual for this type of precipitate, but it demonstrates the structural connection between all the metastable phases in the Al–Mg–Si(–Cu) system through the construction rules and the Si-network.

The precipitate in Figure 12 is also decorating a dislocation line, although its structure is different from the precipitate in Figure 11. It consists of a monoclinic unit indicated by yellow lines in Figure 12, with $4d_{Al}$ (16.20 Å) periodicity along <100>Al. The monoclinic unit contains C subunits indicated by dashed white lines. In addition, the whole structure is mirrored by a mirror plane viewed edge on and indicated by the double line in Figure 12.

4. Discussion

The mechanical properties of the 5005 alloy are significantly changed after a combined deformation and ageing process compared with the conditions without deformation or ageing. This demonstrates that it is possible to significantly increase the strength of an alloy that has previously been considered non-heat-treatable. The standard states that the 5005 alloy can achieve higher strength in some conditions, but the minimum elongation is then significantly lower (less than 4%) than what has been found here [32]. After deformation, the dislocation density is increased, and this both increases the diffusion speed of the alloying elements and acts as nucleation sites for precipitation. In the present work, it is the presence of Si that facilitates the formation of precipitates despite its low concentration of only 0.15 wt%.

The deformation in itself can be seen to greatly increase the yield strength while slightly increasing the ultimate tensile strength, as shown in Tables 2 and 3, but the combination of artificial ageing and deformation shows an even greater increase, as shown in Figure 3. This means that there is a significant strength contribution from both the introduction of dislocations and the increased precipitation density found after artificial ageing.

The initial deformation temperature does not have any impact on the mechanical properties. In this case, the tool was kept at room temperature, which led to the quenching of the material during deformation and, hence, a reduction in dynamic recovery. It is likely that most of the deformed conditions were cooled to a temperature close to room temperature when the deformation ended, and this locked in the dislocations and kept the deformation structure and strength contribution of all these conditions at a similar level. To improve this study, heated tools that could keep the material at the selected temperature during deformation are necessary to clearly determine if the deformation temperature influences the final mechanical properties.

The grain structure and the primary particle distribution are not changed after the deformation, with small to no visible differences between the investigated conditions. The amount of deformation is too low to observe any changes in the optical micrographs that might show up if higher deformations levels were investigated.

The precipitates that are found in the alloy are well known from the 6xxx-series system, but in the IM condition, they are mainly distributed along dislocation lines, indicating a segregation of solute elements to the dislocations that contribute to the increased precipitate density compared with the nondeformed sample. The segregation of the solute elements to the dislocation lines enables them to act as nucleation sites for precipitates with well-defined cross sections and for precipitates that are decorating the dislocation lines. It should be mentioned that all these precipitates are viewed in cross section and extend along the viewing <001>Al directions. The higher precipitate density in the IM condition is increasing its mechanical properties as compared with the undeformed condition. The precipitates in both conditions are typical for the Al–Mg–Si(–Cu) system, built according to

the construction rules given in [6] and containing the well-known Si-network [9]. Many precipitates nucleated on dislocations in the IM condition had interfaces along <100>Al directions that were found to be stabilized by Cu-rich atomic columns forming local C subunits. These interfaces could accommodate various bulk crystal structures, as the precipitates in Figures 9, 11 and 12 show. This is an indication that Cu is important in enhancing the precipitation hardening in predeformed conditions, even when present at low concentrations. It can be observed that the number of Cu-containing columns is very low in the overlaid precipitates in respect to the total number of atomic columns in these precipitates. Most likely, the C subunits stabilize the precipitate interfaces due to the strong covalent bonding between the Cu atomic columns and the nearby Si columns that are part of the Si-network. The C subunits along <100>Al directions tend to form with certain periodicities, such as $3d_{Al}$ (12.15 Å) and $4d_{Al}$ (16.20 Å), also reported in [30], most likely related to strain alleviation when the bulk structure becomes periodic along <100>Al. It is interesting to note that no precipitates with elongated cross sections or with cross sections along <100>Al were observed in the Undef condition, which indicates that the formation of C subunits and the precipitate's interfaces along <100>Al are enhanced by the predeformation.

It is obvious that the low amount of Si present in the alloy is responsible for precipitation in quantities able to increase the mechanical properties. It was expected that such amount was not sufficient to create precipitates and that the alloy would therefore give knowledge about the effect of an isothermal heat treatment on the strength contribution from dislocations, hence indirectly giving information about the dislocation density. Instead, we obtained a significant increase in mechanical properties, and found that the combination of mechanical deformation and isothermal artificial ageing increased the yield strength by more than 120% and the ultimate tensile strength by 50%. We were not able to determine the effect of dislocation density on mechanical properties after deformation, but it can be clearly seen in Figure 7 that there is a significant increase in dislocation density after deformation when compared with the undeformed material. The low Si content in this 5005 alloy allowed for precipitation to occur during deformation, but according to the standard, a content up to 0.3 wt% is allowed for 5005 alloys [33]. In a recycling context, where you are likely to have issues keeping the Si level low, the increased level might be beneficial and cause a strength/ductility increase compared with alloys with lower Si content, thus enabling the use of more postconsumer scrap in the recycled material. In addition, a higher Si content should lower the deformation requirement to obtain precipitation hardening, thus making higher mechanical properties possible.

Due to precipitation strengthening, the main idea of investigating the effect of the isothermal heat treatment on the dislocation annihilation was not feasible and would require a purer alloy without Si where strengthening precipitation is impossible. If any dislocation annihilation has occurred during the artificial ageing, the contribution to mechanical properties is significantly lower than the precipitation strengthening observed in this alloy.

Based on earlier works, it is important to control the amounts of other solute elements (Zn and especially Cu) and make sure that the precipitation of other known phases will not occur [10–12]. This could indicate a future research topic to be studied to determine the effect of the recovery of dislocations during artificial ageing temperatures without any influence of precipitates on the mechanical properties.

5. Conclusions

The mechanical properties of a 5005 alloy can be significantly increased from the as-received condition by applying deformation, followed by isothermal artificial ageing. Increases in yield strength of 120% and in tensile strength of 50% have been achieved. The effect is a combination of dislocation strengthening and precipitation strengthening. The contribution from precipitates in yield strength is at least 18 MPa and does not reduce the ductility. The precipitate density and volume fraction after artificial ageing in this

case are significantly increased as compared with a condition that has not been deformed prior to artificial aging. As the observed precipitate types in both conditions are typical for the Al–Mg–Si(–Cu) system, the precipitation and the increased mechanical properties are attributed to the Si and, to a lower extent, Cu contents in the alloy.

Mechanical properties are significantly increased by only deforming the material, but the combined effect of increased dislocations and increased precipitate density after deformation and artificial ageing has caused the significant increase in mechanical properties. This work clearly demonstrates the strong effect of impurity elements that can alter mechanical properties in specific processes and that both alloy producers and end users should be well aware of.

Author Contributions: Methodology, J.H., O.J., C.D.M. and B.J.M.; formal analysis, J.H., C.D.M. and O.J.; investigation, J.H., C.D.M. and B.J.M.; writing—original draft preparation, J.H.; writing—review and editing, J.H., O.J., C.D.M. and B.J.M. All authors have read and agreed to the published version of the manuscript.

Funding: This research was carried out as part of the NRC-funded BIA-IPN project SUFICCS (Superior Fatigue Stressed Chassis Components) withproject number 295816. The project is owned by Raufoss Technology AS with the following partners: Hydro Aluminium AS, AP&T, SINTEF Manufacturing AS, and SINTEF Industry. The experiments were carried out at SINTEF Manufacturing AS and SINTEF Industry.

Data Availability Statement: The original contributions presented in the study are included in the article, further inquiries can be directed to the corresponding author.

Conflicts of Interest: The authors have no conflict of interest to disclose. All authors have approved the contents of this paper, and we adhere to the Vancouver guidelines for co-authorship. SINTEF Manufacturing AS and SINTEF Industry were research partners in the project and had the role as the principal investigators. The funders had no role in the design of the study; in the collection, analyses, or interpretation of data; in writing of the manuscript; or in the decision to publish the results.

References

1. Zheng, K.; Politis, D.; Wang, L.; Lin, J. A review on forming techniques for manufacturing lightweight complex—Shaped aluminium panel components. *Int. J. Lightweight Mater. Manuf.* **2018**, *1*, 55–80. [CrossRef]
2. Oguocha, I.; Adigun, O.; Yannacopoulos, S. Effect of sensitization heat treatment on properties of Al–Mg alloy AA5083-H116. *J. Mater. Sci.* **2008**, *43*, 4208–4214. [CrossRef]
3. Baruah, M.; Borah, A. Processing and Precipitation Strengthening of 6xxx Series Aluminium Alloys: A Review. *Int. J. Mater. Sci.* **2020**, *1*, 40–48. [CrossRef]
4. Meyruey, G.; Massardier, V.; Lefebvre, W.; Perez, M. Over-ageing of an Al-Mg-Si alloy with silicon excess. *Mater. Sci. Eng. A* **2018**, *730*, 92–105. [CrossRef]
5. Marioara, C.; Andersen, S.; Zandbergen, H.; Holmestad, R. The influence of alloy composition on precipitates of the Al-Mg-Si system. *Metall. Mater. Trans. A* **2005**, *36*, 691–702.
6. Andersen, S.; Marioara, C.; Bjørge, R.; Du, Q.; Ringdalen, I.; Wenner, S.; Mørtsell, E.; Holmestad, R.; Saito, T.; Røyset, J.; et al. Directionality and Column Arrangement Principles of Precipitates in Al-Mg-Si-(Cu) and Al-Mg-Cu Linked to Line Defect in Al. *Mater. Sci. Forum* **2016**, *877*, 461–470. [CrossRef]
7. Andersen, S.; Marioara, C.; Friis, J.; Wenner, S.; Holmestad, R. Precipitates in aluminium alloys. *Adv. Phys. X* **2018**, *3*, 1479984. [CrossRef]
8. Sunde, J.; Marioara, C.; Holmestad, R. The effect of low Cu additions on precipitate crystal structures in overaged Al-Mg-Si(-Cu) alloys. *Mater. Charact.* **2020**, *160*, 110087. [CrossRef]
9. Andersen, S.; Marioara, C.; Vissers, R.; Frøseth, A.; Zandbergen, H. The structural relation between precipitates in Al–Mg–Si alloys, the Al-matrix and diamond silicon, with emphasis on the trigonal phase U1-$MgAl_2Si_2$. *Mater. Sci. Eng. A* **2007**, *444*, 157–169. [CrossRef]
10. Zhang, H.; Gue, G.; Li, S.; Li, B.; Nagaumi, H. Influence of cold pre-deformation on the microstructure, mechanical properties and corrosion resistance of Zn-bearing 5xxx aluminum alloy. *J. Mater. Res. Technol.* **2022**, *16*, 1202–1212. [CrossRef]
11. Gue, C.; Chen, Y.; Zhang, H.; Ji, H.; Wu, Z.; Liu, X.; Nagaumi, H. Synchronous improvement of mechanical properties and corrosion resistance of novel heat-treatable 5xxx aluminum alloy by non-isothermal ageing. *J. Alloys Compd.* **2023**, *939*, 168770. [CrossRef]
12. Medrano, S.; Zhao, H.; De Geuser, F.; Gault, B.; Stephenson, L.; Deschamps, A.; Ponge, D.; Raabe, D.; Sinclair, C. Cluster hardening in Al-3Mg triggered by small Cu additions. *Acta Mater.* **2018**, *161*, 12–20. [CrossRef]

13. Sha, G.; Marceau, R.; Gao, X.; Muddle, B.; Ringer, S. Nanostructure of aluminium alloy 2024: Segregation, clustering and precipitation processes. *Acta Mater.* **2011**, *59*, 1659–1670. [CrossRef]
14. Li, J.; Dang, J. A Summary of Corrosion Properties of Al-Rich Solid Solution and Secondary Phase Particles in Al Alloys. *Metals* **2017**, *7*, 84. [CrossRef]
15. Zhang, R.; Knight, S.; Holtz, R.; Goswami, R.; Davies, C.; Birbilis, N. A survey of Sensitization in 5xxx Series Aluminum Alloys. *Corrosion* **2016**, *72*, 144–159. [CrossRef]
16. D'Antuono, D.S.; Gaies, J.; Golumbfskie, W.; Taheri, M. Direct measurement of the effect of cold rolling on β phase precipitation kinetics in 5xxx series aluminum alloys. *Acta Mater.* **2017**, *123*, 264–271.
17. Yi, G.; Zeng, W.; Poplawsky, J.; Cullen, D.; Wang, Z.; Free, M. Characterizing and modeling the precipitation of Mg-rich phases in Al 5xxx alloys aged at low temperatures. *J. Mater. Sci. Technol.* **2017**, *33*, 991–1003. [CrossRef]
18. Xie, J.; Liang, Y.; Yan, F.; Zhou, J.; Du, P.; Liu, W. Effect of high-pressure heat treatment on the recrystallization and recrystallization texture of CC 5005 aluminum alloy. *J. Mater. Res. Technol.* **2023**, *26*, 2017–2027. [CrossRef]
19. Sidor, J.; Chakravarty, P.; Bátorfi, J.; Nagy, P.; Xie, Q.; Gubicza, J. Assessment of Dislocation Density by Various Techniques in Cold Rolled 1050 Aluminum Alloy. *Metals* **2021**, *11*, 1571. [CrossRef]
20. Ashby, M. The deformation of plastically non-homogeneous materials. *Philos. Mag. A J. Theor. Exp. Appl. Phys.* **1970**, *21*, 399–424. [CrossRef]
21. Gruber, B.; Weißensteiner, I.; Kremmer, T.; Grabner, F.; Falkinger, G.; Schökel, A.; Spieckermann, F.; Schäublin, R.; Uggowitzer, P.; Pogatscher, S. Mechanism of low temperature deformation in aluminium alloys. *Mater. Sci. Eng. A* **2020**, *795*, 139935. [CrossRef]
22. Ghosh, M.; Miroux, A.; Kestens, L. Experimental study and modelling of the role of solutes, precipitates and temperature on the work-hardening of AA6xxx aluminium alloys. *Mater. Sci. Eng. A* **2021**, *805*, 140615. [CrossRef]
23. Khadyko, M.; Myhr, O.; Dumoulin, S.; Hopperstad, O. A microstructure-based yield stress and work-hardening model for textured 6xxx aluminium alloys. *Philos. Mag.* **2016**, *96*, 1047–1072. [CrossRef]
24. Lin, J.; Dean, T.; Garrett, R.; Foster, A. Process for Forming Metal Alloy Sheet Components. WO 2008/059242 A2, 22 May 2008.
25. Yi, L.; Yu, G.; Tang, Z.; Li, X.; Gu, Z. Investigation of the Hot Stamping-in-Die Quenching Composite Forming Process of 5083 Aluminum Alloy Skin. *Materials* **2023**, *16*, 2742. [CrossRef]
26. Jiang, H.; Xing, H.; Xu, Z.; Yang, B.; Feng, W.; Sui, T.; Han, Y.; Zhang, J.; Baode, S. Effect of pre-aging and precipitation behavior on mechanical properties of 7055 aluminum alloy processed by hot-forming quenching. *Mater. Charact.* **2023**, *198*, 112729. [CrossRef]
27. Jiang, Y.; Ding, H. Investigations into Hot Form Quench Conditions on Microstructure Evolution and Bake-Hardening Response for High-Strength Aluminum Alloy. *J. Mater. Eng. Perform.* **2020**, *29*, 8331–8339. [CrossRef]
28. *EN-ISO 6982-1:2019*; Metallic Materials-Tensile Testing Part 1: Method of test at room temperature. The European Committee for Standardization: Brussels, Belgium, 2019.
29. Vissers, R.; van Huis, M.; Jansen, J.; Zandbergen, H.; Marioara, C.; Andersen, S. The crystal structure of the β′ phase in Al–Mg–Si alloys. *Acta Mater.* **2007**, *55*, 3815–3823. [CrossRef]
30. Weng, Y.; Jia, Z.; Ding, L.; Du, K.; Duan, H.; Liu, Q.; Wu, X. Special segregation of Cu on the habit plane of lath-like β′ and QP2 precipitates in Al-Mg-Si-Cu alloys. *Scr. Mater.* **2018**, *151*, 33–37. [CrossRef]
31. Marioara, C.; Nakamura, J.; Matsuda, K.; Andersen, S.; Holmestad, R.; Sato, T.; Kawabata, T.; Ikeno, S. HAADF-STEM study of β′-type precipitates in an over-aged Al–Mg–Si–Ag alloy. *Philos. Mag.* **2012**, *92*, 1149–1158. [CrossRef]
32. *EN 485-2:2016*; Aluminium and Aluminium Alloys—Sheet, Strip and Plate—Part 2: Mechanical Properties. The European Committee for Standardization: Brussels, Belgium, 2016.
33. *EN 573-3:2019*; Aluminium and Aluminium Alloys—Chemical Composition and Form of Wrought Products—Part 3: Chemical Composition and Form of Products. The European Committee for Standardization: Brussels, Belgium, 2019.